

# Image Registration of Dynamic MRI for Strain Analysis of Soft Tissue Structures in the Knee Joint using Elastix

Andres M. Arias-Lorza<sup>a,\*</sup>, <sup>~ a</sup>, <sup>~ a</sup>, <sup>~ b,c</sup>, <sup>~ d</sup>, <sup>~ d</sup>, <sup>~ b</sup>, <sup>~ a</sup>

<sup>a</sup>~,  
<sup>b</sup>~,  
<sup>c</sup>~,  
<sup>d</sup>~,

---

## Abstract

MRI is a well established imaging technique for in-vivo studies of human musculoskeletal structures in biomechanics and orthopedic research. However, it is not ideally suited for a detailed motion analysis of soft tissue, as MRI sequences are not yet capable of capturing 3D data with sufficiently high spatio-temporal resolutions. Therefore, we propose a new registration method based on B-spline transformations using rigid constraints at bones implemented in the `elastix` software tool that combines the temporal information from dynamic MRI with the spatial information from a static HR MRI scan of the same subject. Good registrations were obtained from two datasets. The generated HR dynamic MRI of the knee shows realistic transformations of bones and soft tissues. Dice overlap above 90% and  $\sim 85\%$  at bone and fat pad in most postures; and surface distances at bones below 1mm and fat pad  $\sim 1mm$  were obtained. Tissue deformation were evaluated using the Jacobian determinant. Such HR in-vivo dynamic analysis could pave the way for a better understanding of dynamic behaviour of soft tissue structures, including muscles, tendons, ligaments and menisci in healthy, injured or diseased joints.

---

## 1. Introduction

Knee motion analysis is an important tool in biomechanics and orthopedic research. It is commonly used to study osteoarthritis [1, 2], patellofemoral

---

\*Both authors contributed equally

pain [3] and knee injuries [4]. In addition, it is also used in follow-up treatments such as meniscectomy [5] and arthroplasty [6]. Visualization and quantification of knee joint dynamics are therefore essential for disease diagnosing as well as treatment monitoring and assessment, especially in early phases of the disease when joint tissue deformations are still not well manifested [7].

The methods used for knee motion analysis were initially highly invasive, involving the insertion of probes into patient's legs [8, 9, 10]. Today, generally less invasive imaging techniques, such as radiography [11], fluoroscopy [12], computed tomography [13] up to non-invasive magnetic resonance imaging (MRI) [14, 15, 16, 17, 18, 19, 20] are used to visualize the motion of the knee. MRI, in particular, is the only truly non-invasive imaging method and offers excellent soft tissue contrast that can be controlled by various dedicated acquisition sequences. However, due to its long acquisition times and high susceptibility towards motion artifacts, it can typically only acquire single static images at relatively high spatial resolutions or a series of dynamic images with much lower spatial resolution [15]. Although there are some MRI sequences that could provide both high temporal and spatial resolutions (e.g. CINE-MRI), many repeated moving cycles of the knee ( $> 30$ ) are required to get high quality dynamic images [21], which again increases the acquisition time and may also be a limiting factor for patients that are experiencing pain during movement.

In contrast to CINE-MRI, real-time dynamic MR images can be acquired using a single motion cycle. However, in real-time dynamic MRI a compromise between temporal and spatial resolutions is often required, resulting in images that suffer from streaking artifacts and motion blur [21], substantially limiting the possibility of using real-time dynamic MRI for studying soft tissue structures in motion, such as cartilage, tendons, and ligaments.

To overcome the compromises in image resolution, multiple studies [22, 23, 24, 25] tried approximating real-time dynamic MRI measurements with a series of static MRI scans in different positions. However, such step-wise measurements do not provide sufficient information on joint position and orientation, and therefore cannot be considered a realistic dynamic analysis [26]. Furthermore, the visco-elastic nature of soft tissues could lead to deviations in tissue thickness during dynamic movement which are not properly captured by using static images [7].

In order to perform an accurate dynamic analysis using images of higher resolution and better quality, some researchers combined the information obtained from a low-resolution (LR) dynamic 3D MRI data with a high-

resolution (HR) static 3D MRI pre-scan of the same subject [27, 28, 20, 29, 30]. For instance, Boritkar et al. [27] and Clarke et al. [28] integrated the anatomical structures visible in the HR static MRI into the dynamic MRI of the knee and ankle joints respectively. They first obtained detailed 3D models of the bones from the static HR pre-scan, which they then rigidly registered to each time frame of the dynamic LR image series using an iterative closest point algorithm. In both works only the rigid movement of the bones was analysed. Any assessment of soft tissue structures, such as cartilage that is relevant for the diagnosis of osteoarthritis [7], was not included in these studies. Makki et al. [20] expanded the idea of rigid registration with a log-euclidean polyaffine framework (LEPF) [31, 32] to study the movement of the ankle joint. In LEPF, the rigid registration step is followed by a log-euclidean weighting function, which fuses the local rigid transformations of the bones into a continuous deformation field at each time point. The downside of LEPF is that the weighting function of rigid transformations is only based on the distance to the bones and it does not take into account soft tissue information available in the dynamic MRI data.

Recently, several deep learning methods have also been proposed with the intention to overcome the spatio-temporal limitations of the dynamic MRI. Sarasaen et al. [29] took publicly available static HR MR images of the abdomen, spatially down-sampled them to obtain respective LR versions, and trained a U-Net [33] on the HR-LR image pairs in order to predict the original HR data from the LR images. The U-Net was later fine-tuned on a per-patient basis by using a static image from the respective patient. This per-patient trained U-Net was then used to reconstruct dynamic HR MR images. A similar approach was proposed by Chatterjee et al. [30], who aimed to incorporate the temporal information of the dynamic sequence by using a dual-channel U-Net, where one channel inputs the current time frame and the other one the reconstructed HR image from the previous time frame. Training was performed on static image data of a public database, while the dynamic images were artificially created by applying random elastic transformations. Although both methods show good reconstruction of dynamic MRI data and were also able to consider the deformation of soft tissues, static and dynamic images were obtained using the same MRI protocol, which is not often the case in a clinical setting. In addition, there is no direct way, opposite to the image registration approaches, to track the movement of individual voxels by using these deep learning based methods, which is necessary for strain analysis in soft tissues.

In this work, we propose a new method for in-vivo assessment of deformations in soft tissue structures of a knee in motion using dynamic MRI. Our method combines the temporal information from LR dynamic 3D MRI data acquired using a custom-made knee motion device [34] with the spatial information from HR static 3D MRI pre-scans of the same subject by using an image registration approach which combines rigid and non-rigid B-spline transformations using the Elastix registration framework [35]. By doing so, we aim to obtain realistic translations and rotations of rigid bones but also realistic deformations of the surrounding non-rigid soft tissues. Our method is capable of reconstructing an HR dynamic dataset by sequentially transforming the HR static reference image to match the series of LR dynamic images. Furthermore, it is also capable of mapping HR functional information, such as  $T_2$  relaxation times into the dynamic sequence, which has been proven to be useful for disease diagnosis [7]. We applied our registration method on 4 dynamic MRI datasets. We finally show that the tracking of voxel displacements, which results from image registration, can be directly applied to strain analysis of soft tissues. This is in contrast to deep learning based reconstructions that would require additional post-processing methods such as optical flow after the reconstruction of the HR dynamic image sequence. In comparison to other methods, our method also considers non-rigid voxel displacements of soft tissues, provides a basis for strain analysis in soft tissue, and is not constrained by requiring the same MRI protocol for both static and dynamic image acquisition.

## 2. Materials and Methods

The study was approved by the local ethics committee with all volunteers providing written consent prior to their participation in the experiments. The measurement of all subjects involved in this project is carried out in accordance with the Helsinki Declaration of June 1964 (“Ethical Principles for Medical Research Involving Human Subjects”). Data was collected and stored by Charité Universitätsmedizin Berlin and the Universitätsklinikum Jena. Eleven subjects participated in this study, where each individual was scanned at multiple time points (up to 5).

### 2.1. Static and Dynamic MRI Data Acquisition

Static and dynamic data acquisition was performed with a 3T whole-body MRI scanner (Magnetom Prisma Fit, Siemens Healthineers) using two

multipurpose flexible receiver coils (Variety, NORAS MRI products GmbH). A real-time 3D ultra-short echo-time (UTE) MRI sequence with a radial center-out sampling scheme was used [36]. Besides enabling direct imaging of tissues with short  $T_2^*$  relaxation times such as tendons and ligaments [37], the sequence is highly robust against motion artifacts [38, 39]. Most multi-echo static images of the knee were acquired in a sagittal direction with  $\sim 300$  slices reconstructed to a matrix size of  $\sim 400 \times 300$ , in-plane resolution of  $\sim 1 \times 1 \text{ mm}^2$ , slice thickness of  $\sim 1 \text{ mm}$ , using three TE between 30 and  $9,840 \mu\text{s}$ , TR  $\sim 4000 \mu\text{s}$ , and FA  $\sim 10^\circ$ . Similarly,  $\sim 30$  different postures single echo dynamic images were acquired in most subjects in a sagittal direction with 50 – 160 slices reconstructed to a matrix size between 160 to  $432 \times 57$  to 210, in-plane resolution of  $\sim 2 \times 2 \text{ mm}^2$ , slice thickness of  $\sim 4 \text{ mm}$ , TE  $\sim 50 \mu\text{s}$ , TR  $\sim 1300 \mu\text{s}$ , and FA  $\sim 5^\circ$ .

To guide the knees of the volunteers during dynamic MRI acquisitions, a custom-made knee motion device was used. The device, as shown in Fig. 1, is made out of MRI-compatible materials and is designed to be placed within the bore of the MRI scanner. The aim of the device is to hold the patient’s leg and to prevent motions orthogonal to the plane of normal knee movement, therefore minimizing the undesired out-of-plane motion of the knee joint [34]. The device also allows for both active (participant-driven) and passive (motor-driven) continuous knee motions, as well as for static acquisitions in different locked positions, ranging from full extension to approximately  $40^\circ$  of flexion in the sagittal plane.

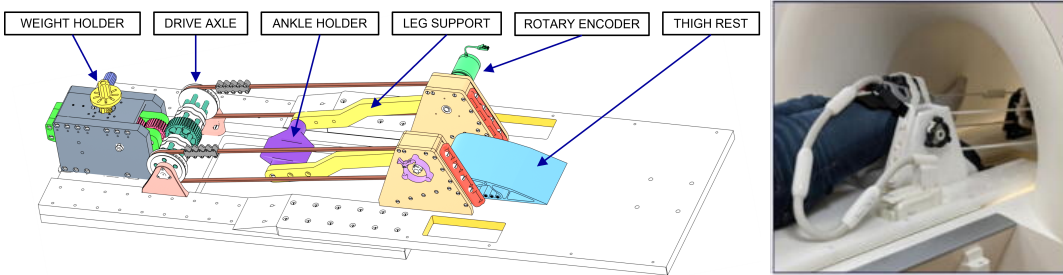


Figure 1: 3D rendering and photograph [34] of the knee motion device which allows active (participant-driven) and passive (motor-driven) motions with/without weight, synchronizing the knee angle with the MRI data.

From the eleven subjects that participated in the study, only two had visits with both static HR and dynamic LR MRI images: subject ID 1 at visit 4, and subject ID 7 at visit 1. Dynamic analysis without static to

dynamic image registration would be possible on subjects IDs: 3 (visits 3 and 4), 4 (visit 2), and 11 (visit 1). Images of those cases are shown in Table 1.

## 2.2. Image Registration Framework

The main idea behind our proposed method is to spatially align the musculoskeletal structures of the knee from the HR images to each time frame of the LR dynamic image series. This approach enables us to combine the spatial image information available in the high-resolution data with the temporal information of dynamic data, and therefore allowing us to describe in detail the motion of soft and rigid tissues from dynamic imaging.

Briefly, image registration is a process of aligning the space of the moving image  $I_M : \Omega_M \subset \mathbb{R}^3 \rightarrow \mathbb{R}$  to the space of the fixed image  $I_F : \Omega_F \subset \mathbb{R}^3 \rightarrow \mathbb{R}$  by finding a transformation  $\mathbf{T} : \Omega_F \rightarrow \Omega_M$  that maps each point of the fixed image space to its corresponding location in the space of the moving image. A transformation  $\mathbf{T}$  could be rigid such that  $\Omega_F$  could be translated, rotated, or scaled; or non-rigid where each point  $\mathbf{x} \in \Omega_F$  can move freely. Often, non-rigid transformations are modeled by B-splines [40], where the transformation is represented by a smooth deformation field based on a grid of control points. Finally, the transformation parameters are found by maximizing a suitable similarity measure  $Sm(I_F, I_M(\mathbf{T}(\Omega_F))) \in \mathbb{R}$  between the transformed moving image and the fixed image.

In this work, the registrations are done using the `elastix` software tool which is widely used in the context of medical image registration [35]. `elastix` is a command line program, where given the fixed image and moving image files represented by `fixedImage` and `movingImage`, the most basic command to run a registration is as follows: `elastix -f fixedImage -m movingImage -out outputDirectory -p parameterFile.txt`, where the output folder is given by `outputDirectory` and `parameterFile.txt` is a text file containing all registration parameter settings such as the transformation type and the kind of similarity measure.

Our registration approach consists of two parts: first, the registration between consecutive images in the LR dynamic MRI; and second, the registration between the HR static MRI and the most similar images in the dynamic series. Then using the obtained transformations, the static images and its segmentations can be propagated forward and backwards in time. This approach is described in Figure 2.

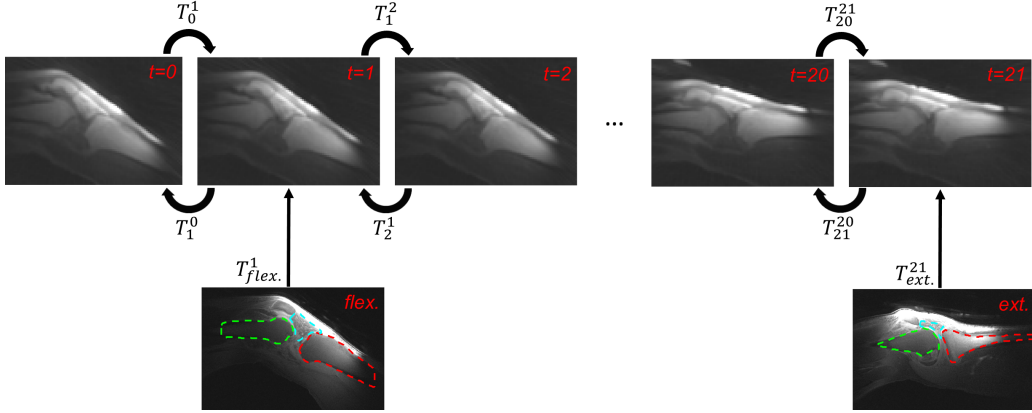
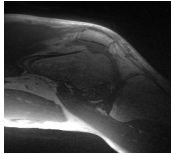
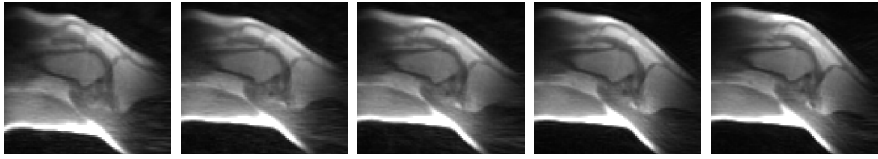

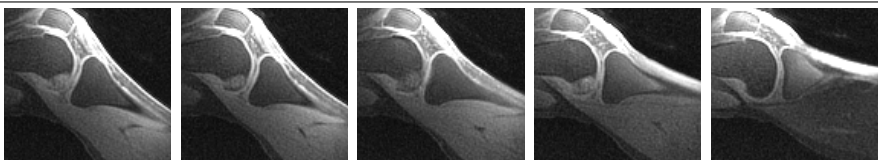
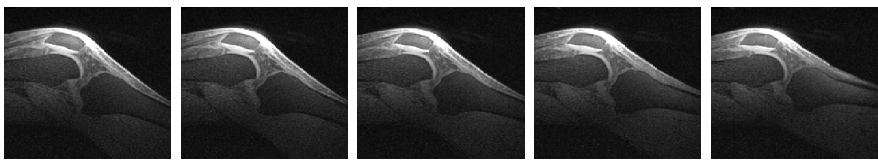
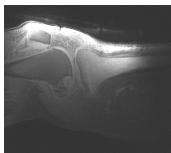
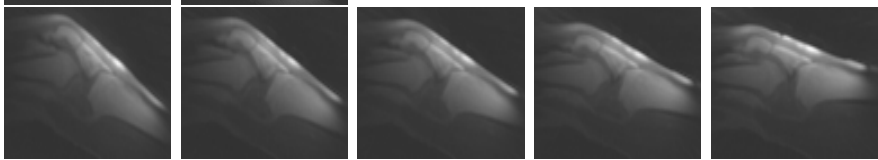
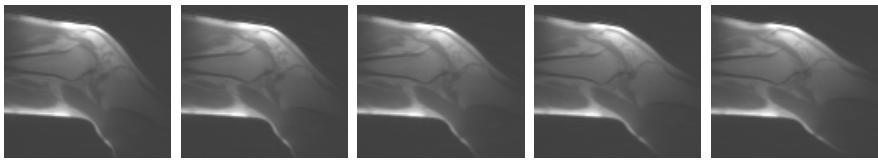


Figure 2: Proposed registration method. Consecutive images in the dynamic series (top) are registered to obtain a transformation ( $T_i^{i+1}$ ) and its inverse ( $T_{i+1}^i$ ). Static HR images (bottom) in flexed (flex.) and extended (ext.) positions are registered to the most similar images in the dynamic series, then these static images and its segmentations can be propagated forward and backwards in time.

### 2.2.1. Dynamic MRI Registration

Given a dynamic MRI series composed of  $n+1$  images:  $I_i^{dyn.} : \Omega_{dyn.} \subset \mathbb{R}^3 \rightarrow \mathbb{R}$  where  $i = [0, \dots, n]$ , for the registration between consecutive images  $I_i^{dyn.}$  and  $I_{i+1}^{dyn.}$ , such that  $I_{i+1}^{dyn.}$  is the fixed image and  $I_i^{dyn.}$  the moving image, we try to find a transformation  $T_i^{i+1}$  that aligns image  $I_i^{dyn.}$  to image  $I_{i+1}^{dyn.}$ . As between consecutive images a small rotation of the tibia bone and small non-rigid deformations of soft tissues are expected, we use non-rigid B-splines transformation, represented in the `elastix` parameter file by: (`Transform "BSplineTransform"`). For the grid control point resolution we searched for a good trade-off between a low computation time plus memory consumption, and a small grid spacing; after trying several grid resolutions (1x, 2x, 3x,... image resolution) we observed a good trade-off in a three voxels grid space represented in the parameter file by: (`FinalGridSpacingInVoxels 3`).

Table 1: Description of available dynamic knee MRI. Postures 1, 5 10, 15, and 20 are shown. A static image is also shown above the dynamic sequence if available. Acquisition parameters are also described: size (x, y, z dimensions, No. postures), resolution, TE, TR, and FA. Note: the dynamic images in subject 1 were acquired in coronal direction but are visualized in sagittal view.

ID	Visit	MRI images	Parameters
1	v4		480 × 400 × 288 0.83 × 0.83 × 1.25mm {30, 2430}μs 5000μs 8°
			192 × 57 × 160 × 24 2.08 × 2.08 × 4.44mm 30μs 1300μs 4°
3	v3		336 × 210 × 152 × 50 1.56 × 1.56 × 1.56mm 55μs 1700μs 5°
	v4		336 × 210 × 152 × 30 1.42 × 1.42 × 1.42mm {55, 2415}μs 4200μs 5°
4	v2		432 × 196 × 270 × 33 1.18 × 1.18 × 1.18mm 55μs 2000μs 5°
7	v1		416 × 378 × 277 × 2 0.86 × 0.86 × 0.86mm {100, 2480, 4860}μs 7300μs 10°
			160 × 100 × 50 × 22 2.25 × 2.25 × 4.5mm 70μs 1000μs 5°
11	v1		192 × 160 × 57 × 25 2.0 × 2.0 × 4.1mm 30μs 1300μs 4°



A finer grid could result in better registration of small non-rigid structures such as the fat pat, but it could also lead to more irregular deformations [35]. Therefore, to get smooth deformations we use a hierarchical approach in the grid resolution. Three resolutions are used, starting by 4 times the in-plane final grid resolution, halving for the subsequent resolutions until the final grid spacing of 3 voxels is reached. As the image between-planes resolution is already quite low ( $\sim 4\text{mm}$ ), the z-dimension of the grid is not affected by the multi-resolution approach. In the parameter file this is defined by: (`GridSpacingSchedule 4 4 1 2 2 1 1 1 1`). The rest of parameters are the same as suggested by `elastix` for B-splines registration.

However, by only using B-splines transformation for the registration between consecutive images does not guarantee the bones being rigidly registered. Therefore, we want  $\mathbf{T}_i^{i+1}$  to be rigid inside bones and non-rigid in soft tissues. In [41], a voxel distance preserving penalty inside rigid regions is presented. The idea is that inside rigid regions the distance between any two voxels should be preserved after an image is transformed by penalizing the differences. Given a rigid region inside image  $I_i^{dyn.}$  ( $\Omega_{R_i} \subset \Omega_{dyn.}$ ) and a rigidity penalization ( $Pm : \mathbb{R}^3 \times \mathbb{R}^3 \rightarrow \mathbb{R}$ ), then finding the transformation  $\mathbf{T}_i^{i+1}$  is given by:

$$\arg \min_{\mathbf{T}_i^{i+1}} \left( -Sm \left( I_{i+1}^{dyn.}, I_i^{dyn.}(\mathbf{T}_i^{i+1}(\Omega_{dyn.})) \right) + \lambda Pm \left( \Omega_{R_i}, \mathbf{T}_i^{i+1}(\Omega_{R_i}) \right) \right),$$

where  $\lambda$  weights the contribution of the rigidity penalization in the optimization process. In the `elastix` parameter file `parameterFile.txt` we specify the two metrics ( $Sm$  and  $Pm$ ) by: (`Metric "AdvancedNormalizedCorrelation" "DistancePreservingRigidityPenalty"`). Normalized correlation is suitable for registering images with similar intensities [35] such as the registration of consecutive images in a dynamic sequence. As suggested by [41], we set  $\lambda = 0.01$  by (`Metric0Weight 1.0`) and (`Metric1Weight 0.01`). The rigid region  $\Omega_{R_i}$  is given by: (`SegmentedImageName "RigidFileI"`), where `RigidFileI` is the bones segmentation file at posture  $i$  where each bone (tibia and femur) are assigned a different label (integer values 1, 2, and 0 for background). Finally, the rigid region spacing in x-y-z dimensions is represented by (`PenaltyGridSpacingInVoxels 1 1 1`) (see Appendix 6.1 for a full description of the parameter file).

To get bones segmentations at each posture, the bones segmentation at posture 0 ( $S_0^{dyn.} : \Omega_{dyn.} \rightarrow \mathbb{Z}$ ) is rigidly register to each posture. To do

this,  $S_0^{dyn.}$  is first propagated to each posture  $i + 1$  to get an approximation of the bones segmentation ( $S_{i+1}^{dyn.}$ ). This is done by applying the obtained transformation  $\mathbf{T}_i^{i+1}$  as:  $S_{i+1}^{dyn.} = S_i^{dyn.}(\mathbf{T}_i^{i+1}(\Omega_{dyn.}))$ . In `elastix` this is implemented as: `transformix -in LabelI_J -out outputDirectoryI+1 -tp outputDirectoryI+1/TransformParameters.0.txt`, where `LabelI_J` is the image file name for each label  $J$  in  $S_i^{dyn.}$ , and `outputDirectoryI+1/TransformParameters.0.txt` the file containing  $\mathbf{T}_i^{i+1}$ . Then as second step, the rigid bones at each posture are obtained by rigidly register  $S_0^{dyn.}$  to each posture  $i$ . This is done by rigidly register each bone in  $S_0^{dyn.}$  to each approximation of the bone segmentation in  $S_i^{dyn.}$ , where the rigid transformation is defined by Euler rigid transform which only allows for rotation and translation. In the `elastix` parameter file this is defined by: (`Transform "EulerTransform"`) (a full description of the rigid registration parameter file is shown in Appendix 6.2).

Further, as the dynamic images could be noisy and contain moving artifacts outside the knee region which could lead to registration errors, to obtain  $\mathbf{T}_i^{i+1}$  we perform the registration only inside a Region of Interest (ROI) around the knee, which is represented by a bounding box to fit the propagated segmented bones at posture  $i$  and then slightly dilated by few voxels to cover possible tissues deformations after registration outside the non-dilated region. In `elastix` this kind of registration is supported by masks.

The computation of  $\mathbf{T}_i^{i+1}$  allows a forward propagation of the static images and segmentations, however as shown in Figure 2 backward propagation may be also needed. Backward transformations can be obtained by computing the inverse of  $\mathbf{T}_i^{i+1}$  by:  $\mathbf{T}_{i+1}^i = Inverse(\mathbf{T}_i^{i+1})$ . This is computed by first transforming the image ( $I_i^{dyn.}(\mathbf{T}_i^{i+1}(\Omega_{dyn.}))$ ) and using it as moving image with the fixed image being  $I_i^{dyn.}$ . In `elastix` this is done as: `elastix -f DynIFile -m DynIFile -out outputDirectoryI+1 -t0 outputDirectoryI+1/TransformParameters.0.txt -p parameterFile.txt`, where `DynIFile` is  $I_i^{dyn.}$  image file, and `parameterFile.txt` is the same file used to get  $\mathbf{T}_i^{i+1}$  but the similarity metric is changed to penalize voxel distances by using (`Metric "DisplacementMagnitudePenalty"`).

### 2.2.2. Static to Dynamic MRI Registration

Static images  $I_j^{stat.} : \Omega_{stat.} \subset \mathbb{R}^3 \rightarrow \mathbb{R}$  where  $j = \{flex., ext.\}$  for flexed and extended positions, are register to the most similar images in the dynamic series  $I_i^{dyn.}$ , as better registration should be expected between similar images.

To find the most similar images, bones segmentations for each static image are registered to the propagated segmented bones on each posture  $i$ . For this, we use a translation only transformation: (`Transform "TranslationTransform"`), as the aim of these registrations is to check how similar the static and dynamic postures are, instead of getting good alignments after registration. Therefore, each static image segmentation  $j$  is translated to all dynamic postures, where the most similar posture is the one with the maximum dice overlap between bones. Then the next step is to get accurate registration between the static images to its most similar dynamic sequence postures. As a composition of rigid and non-rigid deformations could be necessary to register a static to a dynamic image, we first apply an affine registration which allows rigid transformations plus image zooming, followed by a B-spline transform. Also, as the images contrast are very different between static and dynamic images due to differences in acquisition parameters, and properties such as resolution and sizes, this makes the registration by using the intensity information only very challenging. Then instead of performing an intensity-based registration, we register the segmentations of soft and bone tissues which is less challenging to register and better quality registrations would be expected. In `elastix` the registration between static and dynamic segmentations is implemented as: `elastix -f SegDynK -m SegStatJ -out outputDirectory -p ParFileAffine.txt -p ParFileBSpline.txt`, where `SegStatJ` and `SegDynK` are the segmentation image files (tibia, femur, fat pad, and background assigned a different integer value between 0 and 3) for the static image  $j$  and for posture  $k$  in the dynamic image, with postures  $k = \{k1, k2\} \in \mathbb{Z}$  being the most similar to each static image  $j$ ; and `ParFileAffine.txt` and `ParFileBSpline.txt` the parameter files for affine and B-spline registrations. These registrations results in the transformations from the static images  $j$  to the dynamic image  $k$ :  $T_{\{flex.,ext.\}}^k : \Omega_{dyn.} \rightarrow \Omega_{stat.}$ .

Each static images  $j$ , its segmentations and T2 maps can be transformed to postures  $k$  by applying the obtained transformation  $T_{\{flex.,ext.\}}^k$ . T2 maps of the static images are obtained by fitting the signal equation to the multi-echo intensity values. Given the MRI signal  $S$  defined as:  $S = K e^{-TE/T2}$ , where  $K$  is a constant value, by computing  $\log(S)$  the T2 maps can be obtained by

solving the following linear system of equations:

$$\begin{bmatrix} 1 & 0 & \cdots & 0 & TE_1 & 0 & \cdots & 0 \\ \vdots & \vdots & \ddots & \vdots & \vdots & \vdots & \ddots & \vdots \\ 1 & 0 & \cdots & 0 & TE_M & 0 & \cdots & 0 \\ \vdots & \ddots & \ddots & \vdots & \vdots & \ddots & \ddots & \vdots \\ 0 & \cdots & 0 & 1 & 0 & \cdots & 0 & TE_1 \\ \vdots & \ddots & \vdots & \vdots & \vdots & \ddots & \vdots & \vdots \\ 0 & \cdots & 0 & 1 & 0 & \cdots & 0 & TE_M \end{bmatrix} \begin{bmatrix} \log(K_1) \\ \vdots \\ \log(K_N) \\ -1/T2_1 \\ \vdots \\ -1/T2_N \end{bmatrix} = \begin{bmatrix} \log(S_{1,TE_1}) \\ \vdots \\ \log(S_{1,TE_M}) \\ \vdots \\ \log(S_{N,TE_1}) \\ \vdots \\ \log(S_{N,TE_M}) \end{bmatrix},$$

where  $\{TE_1, \dots, TE_M\}$  are the available  $M$  echo times,  $N$  the total number of voxels,  $\{K_1, \dots, K_N\}$  the constant values  $K$  for each voxel,  $\{S_{1,TE_1}, \dots, S_{N,TE_M}\}$  the signal values  $S$  per voxel per echo time, and  $\{T2_1, \dots, T2_N\}$  the T2 value per voxel in the static images. Implementing the above matrices as sparse arrays save memory space and speed up computation by using a least-squares regression algorithm to solve the system of equations.

The transformation of the static images, segmentation, and T2 maps are done with `transformix`. However as the inputs of each transformation  $T_{\{flex.,ext.\}}^k$  is defined in the dynamic image space  $\Omega_{dyn.}$ , the transformation file generated by the `elastix` command needs to be edited such as the resolution is the same as in  $\Omega_{stat.}$ . The resolution of  $\Omega_{stat.}$  in the x-y-z dimension is given by  $(dx_{stat.}, dy_{stat.}, dz_{stat.})$ mm, and the size of the dynamic images represented by  $(Dx_{dyn.}, Dy_{dyn.}, Dz_{dyn.})$ mm, then in the transformation files the input spacing is redefined to the new resolution by: (`Spacing`  $dx_{stat.}$   $dy_{stat.}$   $dz_{stat.}$ ), and the new image size in voxels by: (`Size`  $Dx_{dyn.}/dx_{stat.}$   $Dy_{dyn.}/dy_{stat.}$   $Dz_{dyn.}/dz_{stat.}$ ), rounding the ratios to the closest integers. This is also assuming that the origins and orientations of both  $\Omega_{dyn.}$  and  $\Omega_{stat.}$  are the same.

The transformed HR images are now propagated to the other postures using the transformations between postures  $\mathbf{T}_i^{i+1}$  in case of forward transformation,  $\mathbf{T}_{i+1}^i$  if backward. Again these transformations are implemented by `transformix` and the transformation files should be edited as before to have the resolution of the static images. Finally, in case of multiple-static postures, as described in Figure 2, to get the HR images between the postures  $k1$  and  $k2$ ,  $k1$  posture should be forwardly propagated half number of postures while  $k2$  backwardly propagated.

### 3. Results

To execute the method, in the static HR MRI images and posture 0 in the dynamic MRI, fat pad, femur and tibia bones were manually segmented by a medical imaging researcher (ML) using the medical imaging tool Amira. The two closest dynamic images ( $k1, k2$ ) to the static are also manually segmented. To evaluate the quality of the registration results, we compare the propagation of the static segmentations in the dynamic MRI sequence to manual annotations done on each posture in the LR sequence by two observers (ML (Obs.1), AA (Obs.2)). Comparisons were done using dice overlapping (DSC) and median surface distances. Additionally, we evaluate tissue deformations on the reconstructed HR dynamic MRI by using the Jacobian determinant  $|J(\mathbf{x})| = |[\nabla \mathbf{T}_x(\mathbf{x}), \nabla \mathbf{T}_y(\mathbf{x}), \nabla \mathbf{T}_z(\mathbf{x})]^T|$ , where each row of  $J$  at voxel  $\mathbf{x}$  is the gradient of the transformation  $\mathbf{T}$  on each dimension  $x, y, z$ . An interesting property of the determinant of  $J$  is that it is equivalent to a volume change ratio at each point  $\mathbf{x}$  ( $|J(\mathbf{x})| \equiv Volume(\mathbf{T}(\mathbf{x}))/Volume(\mathbf{x})$ ), therefore if  $|J(\mathbf{x})| = 1$  the volume at  $\mathbf{x}$  after the transformation  $\mathbf{T}(\mathbf{x})$  is preserved such as in rigid deformations, if  $|J(\mathbf{x})| < 1$  there was compression, and if  $|J(\mathbf{x})| > 1$  a volume expansion. As  $\mathbf{T}_i^{i+1}$  maps each point from the fixed to the moving image, then to get the volume deformation from the moving to fixed image the inverse of the Jacobian determinant is used instead as:  $|\mathbf{J}(\mathbf{T}_i^{i+1}(\Omega_{dyn.}))|^{-1}$ . The Jacobian determinant of  $\mathbf{T}_i^{i+1}$  is computed in `elastix` by applying the command `transformix -jac all` in the HR edited file of  $\mathbf{T}_i^{i+1}$ .

Registration results for subject 7 are shown in Figure 3. HR dynamic sequences are obtained for each echo time image, T2 maps, and Jacobians. The segmentations done in the static HR images are also propagated in the HR dynamic sequence. Registered images and segmentations look realistic with bones conserving their shape across the sequence, and fat pad compressing and stretching. Good contrast of different tissues are observed in the T2 maps even better than the different echo time images, for instance tendons are clearly visible. The inverse of Jacobian determinant ( $|\mathbf{J}|^{-1}$ ) is  $\sim 1$  at bones suggesting rigid deformations, while most voxels in fat pad  $< 1$  suggesting volume compression. Quantifications of the registration quality are described in Figure 4. The static segmentations are propagated to each posture in LR and compared to each observer by DSC and surface distance. DSC and distances for tibia and fat pad between registered segmentations and Obs.1 are comparable ( $p > 0.01$  Wilcoxon test) to between observers.

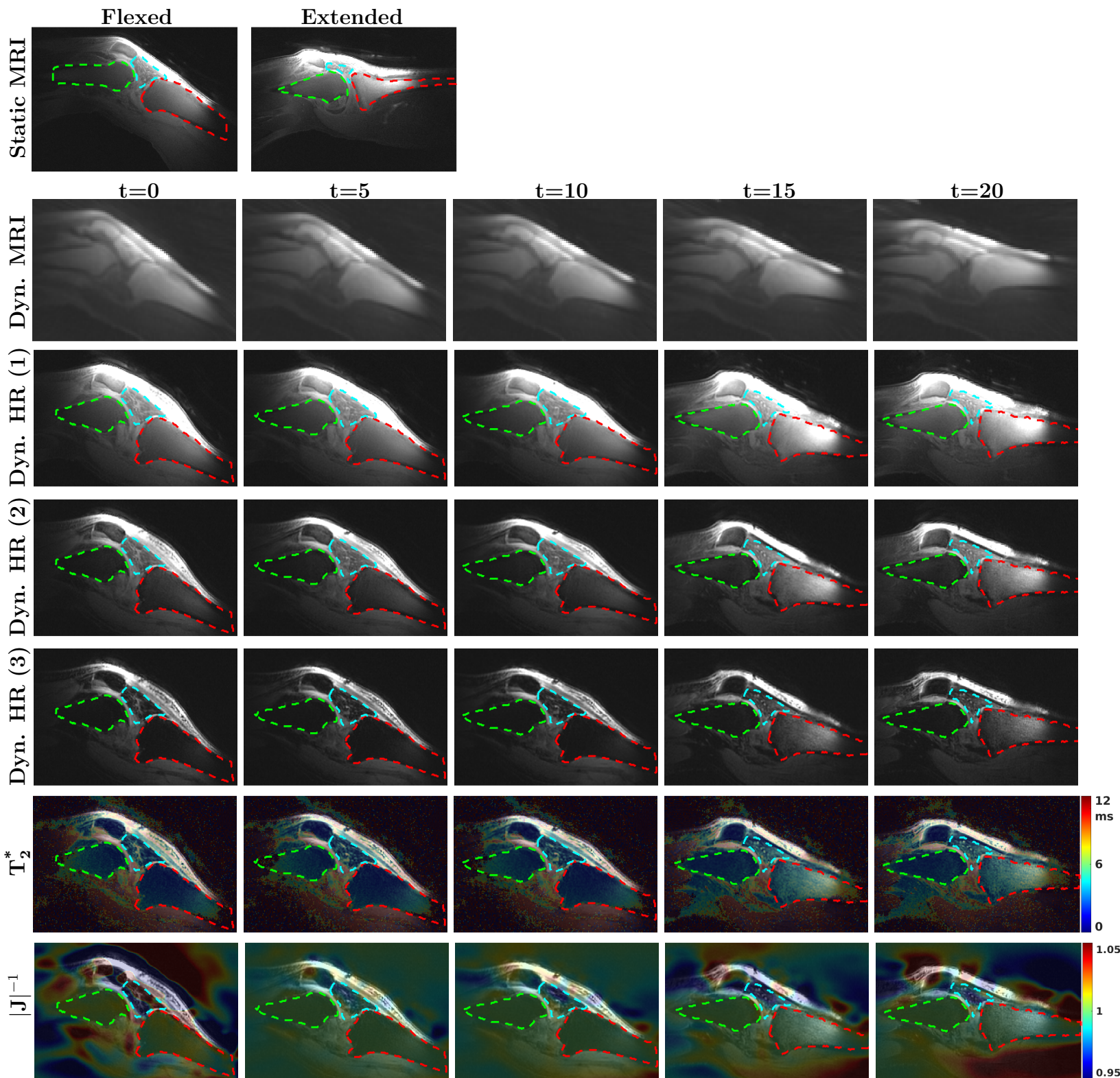


Figure 3: Registration results on Subject 7. Static HR images (row 1) and its segmentations (green contour: femur, red: tibia, blue: fat pad) are registered to the LR dynamic sequence (row 2), resulting in a HR dynamic sequence for each echo time (0.1, 2.48, and 4.86ms) (rows 3-5) with its registered segmentations. HR  $T_2^*$  maps (row 6) and inverse Jacobian determinant of  $\mathbf{T}_i^{i+1}$  (row 7) are also shown.

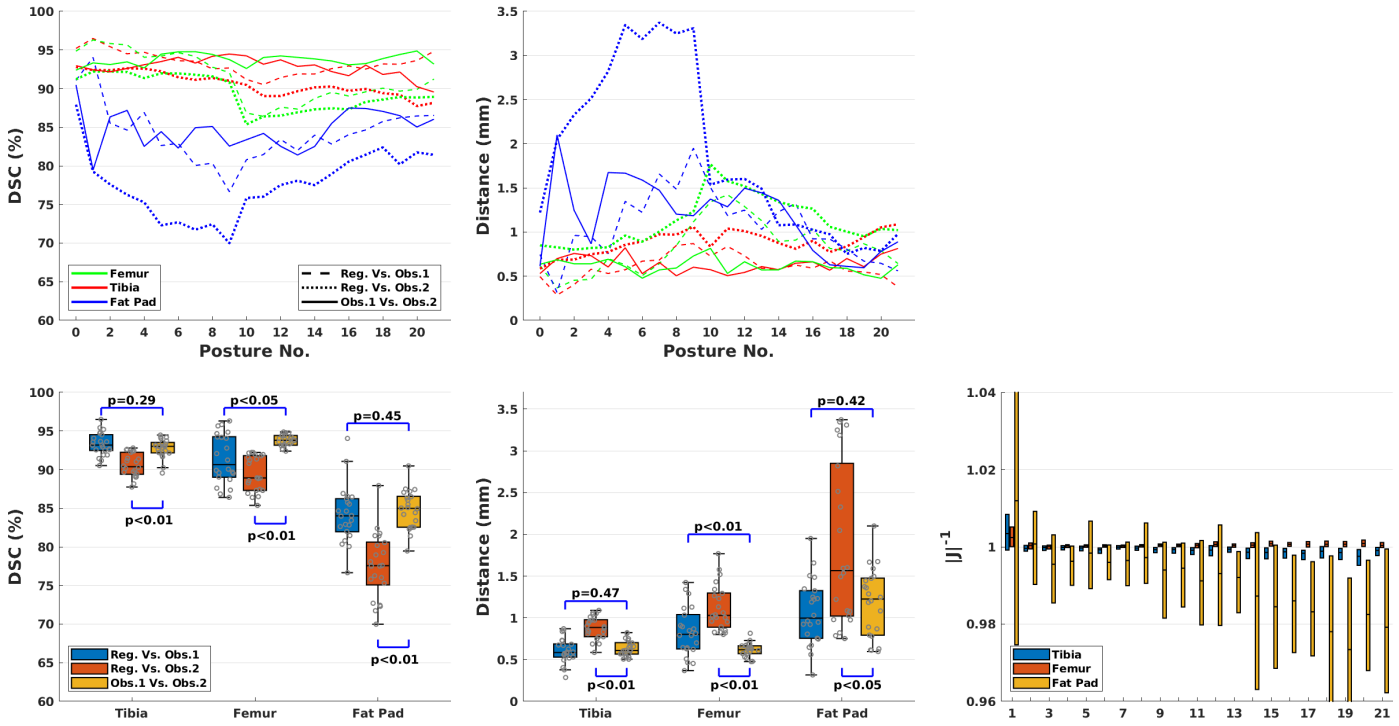


Figure 4: Quantification of registration performance. Top: DSC and surface distances per posture between the registered static segmentations and manual annotations done by two observers, and the DSC and distances between observers. Bottom (left and center): Box plots of DSC and surface distances where each box contains all posture measurements. Median values are compared to the inter-observer medians by Wilcoxon test. Bottom right: Box plot of the inverse of Jacobian determinant values per posture per tissue annotated by Obs.1 (whiskers not show to improve visualization).

It is also observed a decay in registration performance in the middle postures due error propagation, while the highest performances are generally observed at the postures closest to the static images (postures 1 and 21). For most postures the distances between registered segmentations and Obs.1 are much below the dynamic image resolution ( $2.25 \times 2.25 \times 4.5mm$ ). The inverse of the Jacobian determinant voxel values per tissue annotated by Obs.1 for each posture are also shown in Figure 4. As expected bone values are  $\sim 1$ , while most values in the fat pat are  $< 1$ , although a small shift is also observed in the latest posture which could be due to the error propagation.

## 4. Discussion

In this work, we present a method to get a dynamic HR MRI sequence of the knee movement which could be used to analyse the deformations and strain analysis of soft tissues. To do this, we developed a registration method based on the software tool `elastix`. The method registers HR static images with a real time LR dynamic sequence obtained with customized motion device, allowing to merge the HR spatial information from the static images with the temporal information of the dynamic sequence. The registration results in a series of transformations that could be used to get a HR MRI sequence but also to get HR dynamic parameter maps such as T2 and Jacobian determinant maps. These transformations can be also used to track the deformations of tissues segmented in the HR static images. For instance in the static images and HR T2 maps, tissues such as fat pad, and tendons are much better visualized than in the LR MRI, then deformations of these tissues could be better analyzed by using the registrations.

The method generated high quality registrations. The presented non-rigid registration approach including rigid constraints at bones permitted to get realistic deformations with rigid transformations in the bones, and non-rigid deformations in soft tissues, which were observed in the registered HR images and validated using the Jacobian determinant. We evaluated the registrations quality by comparing the transformed HR static segmentation to manual segmentations done in the dynamic sequence. Good results were obtained with dice overlap above 90% at bone, and  $\sim 85\%$  in fat pad in most postures. Surface distances at bones were below 1mm and fat pad  $\sim 1mm$  much shorter than the LR image resolution. Both dices and surface distances for tibia and fat pad were comparable to the inter-observer variability, demonstrating the propagated segmentation being as good as manual observers. However, we observed that better comparisons were obtained with respect to the annotations from Obs.1 than with Obs.2. This could be due to the segmentations inputs in the registration approach were done by Obs.1 biasing the transformed segmentations to that observer. It is also observed that the registered femur is not being comparable to the inter-observer variability. A possible reason the femur being over-segmented in the static images. The intensity non-uniformity common in 3T MRI, which is more noticeable at the borders of the image which is located part of the femur can make the manual annotations a challenging task. Further, we also observed that there is a decay in registration quality after applying several transformations due to



error propagation. A source of error could be due to the image interpolation after applying a transformation to get the registered image. A succession of this sequence of transformation then interpolation can lead to the propagation of the interpolation errors. To prevent this, composing the series of transformations without intermediate image interpolations could contribute to decrease the error propagation, however in our experiments this did not work. A possible reason could be numerical problems by composing a sequence of highly complex B-spline transformations. In this work, to reduce the error propagation we incorporated several static HR images at different postures in the registration approach.

To analyze the deformations of soft tissue in the HR sequence, we used the Jacobian determinant. By using this we observed compression of most part of the fat pad during flexed to extended movement in a healthy subject. We believe this registration approach could be used to compare Jacobian determinant distributions at different soft tissues between healthy and diseased population during dynamic movement to identify possible bio-markers of early knee disease. Similar could be done with T2 distributions values in soft tissues, which has been shown in the past to be relevant in knee diseases [7]. Other approaches could be done to analyse the deformations. For instance, getting shape representations of soft tissues, and then finding possible correlations in shape dynamics to disease.

There have been other similar methods in the past based on image registration to obtain a HR dynamic MRI sequence. Boritkar et al. [27] reported errors below to 1mm for the patella and femur bones, and Clarke et al. [28] reported a difference of 1.5mm between physical and MRI measurements of moment arms of the ankle angle. Makki et al. [20] reported dices above 90% for several ankle bones without a noticeable decay after postures. The reported errors of Boritkar et al. [27] and Makki et al. [20] are similar to the reported in this work for the knee joint bones, however in the presented method and evaluation soft tissues of the knee were considered. Methods based on deep learning have been also presented [29, 30], although the presented dynamic HR results were good, static and dynamic images were considered from the same MRI protocol which was not the case with our data and often not the case in clinical settings. Another problem with deep learning based methods is that they do not output transformations or deformations fields that could be used to track the movement of individual voxels which is necessary for dynamic analysis in soft tissues.

A drawback in the presented method is the need to segment maximum

three postures of the dynamic MRI images, and the segmentation of all static images. Manual segmentations could introduce errors as observed for the femur due to the intensity bias, but also time consuming. We tried a fully automatic registration approach without getting good results due to the big differences between static and dynamic images. Also the segmentation of bones in the first posture was necessary to apply the rigid constraints in the dynamic registration. In the future, automatic segmentation approaches such as the NN-UNet [42] which has been shown to be very successful in segmentation tasks could be used to segment the knee bones in the dynamic and static MRI, skipping the need of manual segmentations.

In summary, the presented method was successful to get good quality HR dynamic MRI of the knee joint, also it could be used to get HR dynamic parametric maps such as T2 and Jacobian determinant, and finally, this approach can be used to analyse soft tissue deformations. Such HR in-vivo dynamic analysis could pave the way for a better understanding of dynamic behaviour of soft tissue structures, including muscles, tendons, ligaments and menisci in healthy, injured or diseased joints.

## 5. Acknowledgements

~

## 6. Appendix

### 6.1. B-spline with rigid penalty transform parameter file

```
(FixedInternalImagePixelType "float")
(MovingInternalImagePixelType "float")
(UseDirectionCosines "true")
// ***** Main Components *****
(Registration "MultiMetricMultiResolutionRegistration")
(Interpolator "BSplineInterpolator")
(ResampleInterpolator "FinalBSplineInterpolator")
(Resampler "DefaultResampler")
(FixedImagePyramid "FixedSmoothingImagePyramid")
(MovingImagePyramid "MovingSmoothingImagePyramid")
(Optimizer "AdaptiveStochasticGradientDescent")
(Transform "BSplineTransform")
(Metric0Weight 1.0)
(Metric1Weight 0.01)
(Metric "AdvancedNormalizedCorrelation" "DistancePreservingRigidityPenalty")
(SegmentedImageName "RigidFile")
(PenaltyGridSpacingInVoxels 1 1 1)
// ***** Transformation *****
(FinalGridSpacingInVoxels 3)
(HowToCombineTransforms "Compose")
(AutomaticTransformInitialization "false")
// ***** Similarity measure *****
(ErodeMask "false")
// ***** Multiresolution *****
(NumberOfResolutions 3)
(GridSpacingSchedule 4 4 1 2 2 1 1 1)
// ***** Optimizer *****
(MaximumNumberOfIterations 2048)
(MaximumStepLength 0.01)
// ***** Image sampling *****
```

```

(NewSamplesEveryIteration "true")
(ImageSampler "RandomCoordinate")
// ***** Interpolation and Resampling *****
(BSplineInterpolationOrder 1)
(FinalBSplineInterpolationOrder 3)
(DefaultPixelValue 0)
(WriteResultImage "true")
(ResultImagePixelFormat "float")
(ResultImageFormat "nii")

```

## 6.2. Euler transform parameter file

```

(FixedInternalImagePixelFormat "float")
(MovingInternalImagePixelFormat "float")
(UseDirectionCosines "true")
// ***** Main Components *****
(Registration "MultiResolutionRegistration")
(Interpolator "BSplineInterpolator")
(ResampleInterpolator "FinalBSplineInterpolator")
(Resampler "DefaultResampler")
(FixedImagePyramid "FixedRecursiveImagePyramid")
(MovingImagePyramid "MovingRecursiveImagePyramid")
(Optimizer "AdaptiveStochasticGradientDescent")
(Transform "EulerTransform")
(Metric "AdvancedMattesMutualInformation")
// ***** Transformation *****
(AutomaticScalesEstimation "true")
(AutomaticTransformInitialization "true")
(HowToCombineTransforms "Compose")
// ***** Similarity measure *****
(NumberOfHistogramBins 32)
(ErodeMask "false")
// ***** Multiresolution *****
(NumberOfResolutions 4)
// ***** Optimizer *****
(MaximumNumberOfIterations 250)
// ***** Image sampling *****

```

```

(NumberOfSpatialSamples 2048)
(NewSamplesEveryIteration "true")
(ImageSampler "Random")
// ***** Interpolation and Resampling *****
(BSplineInterpolationOrder 1)
(FinalBSplineInterpolationOrder 0)
(DefaultPixelValue 0)
(WriteResultImage "true")
(ResultImagePixelFormat "float")
(ResultImageFormat "nii")

```

## References

- [1] T. P. Andriacchi, A. Mündermann, The role of ambulatory mechanics in the initiation and progression of knee osteoarthritis, *Current opinion in rheumatology* 18 (5) (2006) 514–518.
- [2] P. Kannus, M. Järvinen, Posttraumatic anterior cruciate ligament insufficiency as a cause of osteoarthritis in a knee joint, *Clinical rheumatology* 8 (2) (1989) 251–260.
- [3] C. LaBella, Patellofemoral pain syndrome: evaluation and treatment, *Primary Care: Clinics in office practice* 31 (4) (2004) 977–1003.
- [4] C. Yang, Y. Tashiro, A. Lynch, F. Fu, W. Anderst, Kinematics and arthrokinematics in the chronic acl-deficient knee are altered even in the absence of instability symptoms, *Knee Surgery, Sports Traumatology, Arthroscopy* 26 (5) (2018) 1406–1413.
- [5] L. Zheng, R. Carey, E. Thorhauer, S. Tashman, C. Harner, X. Zhang, In vivo tibiofemoral skeletal kinematics and cartilage contact arthrokinematics during decline walking after isolated meniscectomy, *Medical engineering & physics* 51 (2018) 41–48.
- [6] M. R. Angerame, D. C. Holst, J. M. Jennings, R. D. Komistek, D. A. Dennis, Total knee arthroplasty kinematics, *The Journal of Arthroplasty* 34 (10) (2019) 2502–2510.
- [7] C. P. Neu, Functional imaging in oa: role of imaging in the evaluation of tissue biomechanics, *Osteoarthritis and Cartilage* 22 (10) (2014) 1349–1359.

- [8] M. Lafortune, P. Cavanagh, H. Sommer III, A. Kalenak, Foot inversion-eversion and knee kinematics during walking, *Journal of orthopaedic research* 12 (3) (1994) 412–420.
- [9] A. Van Kampen, R. Huiskes, The three-dimensional tracking pattern of the human patella, *Journal of Orthopaedic Research* 8 (3) (1990) 372–382.
- [10] K. Manal, I. McClay, S. Stanhope, J. Richards, B. Galinat, Comparison of surface mounted markers and attachment methods in estimating tibial rotations during walking: an in vivo study, *Gait & posture* 11 (1) (2000) 38–45.
- [11] B.-M. You, P. Siy, W. Anderst, S. Tashman, In vivo measurement of 3-d skeletal kinematics from sequences of biplane radiographs: application to knee kinematics, *IEEE transactions on medical imaging* 20 (6) (2001) 514–525.
- [12] T. S. Tang, N. MacIntyre, H. Gill, R. Fellows, N. Hill, D. Wilson, R. E. Ellis, Accurate assessment of patellar tracking using fiducial and intensity-based fluoroscopic techniques, *Medical image analysis* 8 (3) (2004) 343–351.
- [13] D. Forsberg, M. Lindblom, P. Quick, H. Gauffin, Quantitative analysis of the patellofemoral motion pattern using semi-automatic processing of 4d ct data, *International journal of computer assisted radiology and surgery* 11 (9) (2016) 1731–1741.
- [14] C. M. Powers, F. G. Shellock, M. Pfaff, Quantification of patellar tracking using kinematic mri, *Journal of Magnetic Resonance Imaging* 8 (3) (1998) 724–732.
- [15] F. Sheehan, R. Smith, 3D musculoskeletal kinematics using dynamic MRI, *Handbook of human motion*. Cham: Springer International Publishing (2017) 1–17.
- [16] A. J. Rebmann, F. T. Sheehan, Precise 3d skeletal kinematics using fast phase contrast magnetic resonance imaging, *Journal of Magnetic Resonance Imaging* 17 (2) (2003) 206–213.

- [17] J. Kaiser, A. Monawer, R. Chaudhary, K. M. Johnson, O. Wieben, R. Kijowski, D. G. Thelen, Accuracy of model-based tracking of knee kinematics and cartilage contact measured by dynamic volumetric mri, *Medical engineering & physics* 38 (10) (2016) 1131–1135.
- [18] J. M. Kaiser, M. F. Vignos, R. Kijowski, G. Baer, D. G. Thelen, Effect of loading on in vivo tibiofemoral and patellofemoral kinematics of healthy and acl-reconstructed knees, *The American journal of sports medicine* 45 (14) (2017) 3272–3279.
- [19] C. E. Draper, J. M. Santos, L. C. Kourtis, T. F. Besier, M. Fredericson, G. S. Beaupre, G. E. Gold, S. L. Delp, Feasibility of using real-time mri to measure joint kinematics in 1.5 t and open-bore 0.5 t systems, *Journal of Magnetic Resonance Imaging: An Official Journal of the International Society for Magnetic Resonance in Medicine* 28 (1) (2008) 158–166.
- [20] K. Makki, B. Borotikar, M. Garetier, S. Brochard, D. B. Salem, F. Rousseau, In vivo ankle joint kinematics from dynamic magnetic resonance imaging using a registration-based framework, *Journal of Biomechanics* 86 (2019) 193–203.
- [21] M. Aleksiev, M. Kraemer, N. M. Brisson, M. B. Maggioni, G. N. Duda, J. R. Reichenbach, High-resolution cine imaging of active guided knee motion using continuously acquired golden-angle radial mri and rotary sensor information, *Magnetic Resonance Imaging* 92 (2022) 161–168.
- [22] R. von Eisenhart-Rothe, M. Siebert, C. Bringmann, T. Vogl, K.-H. Englmeier, H. Graichen, A new in vivo technique for determination of 3d kinematics and contact areas of the patello-femoral and tibio-femoral joint, *Journal of biomechanics* 37 (6) (2004) 927–934.
- [23] R. von Eisenhart-Rothe, U. Lenze, S. Hinterwimmer, F. Pohlig, H. Graichen, T. Stein, F. Welsch, R. Burgkart, Tibiofemoral and patellofemoral joint 3d-kinematics in patients with posterior cruciate ligament deficiency compared to healthy volunteers, *BMC musculoskeletal disorders* 13 (1) (2012) 1–8.
- [24] V. V. Patel, K. Hall, M. Ries, J. Lotz, E. Ozhinsky, C. Lindsey, Y. Lu, S. Majumdar, A three-dimensional mri analysis of knee kinematics, *Journal of Orthopaedic Research* 22 (2) (2004) 283–292.

- [25] V. Vedi, E. Spouse, A. Williams, S. Tennant, D. Hunt, W. Gedroyc, Meniscal movement: an in-vivo study using dynamic mri, *The Journal of bone and joint surgery. British* volume 81 (1) (1999) 37–41.
- [26] A. G. d’Entremont, J. A. Nordmeyer-Massner, C. Bos, D. R. Wilson, K. P. Pruessmann, Do dynamic-based mr knee kinematics methods produce the same results as static methods?, *Magnetic resonance in medicine* 69 (6) (2013) 1634–1644.
- [27] B. S. Borotikar, W. H. Sipprell III, E. E. Wible, F. T. Sheehan, A methodology to accurately quantify patellofemoral cartilage contact kinematics by combining 3d image shape registration and cine-pc mri velocity data, *Journal of biomechanics* 45 (6) (2012) 1117–1122.
- [28] E. Clarke, J. Martin, A. G. d’Entremont, M. Pandy, D. R. Wilson, R. Herbert, A non-invasive, 3d, dynamic mri method for measuring muscle moment arms in vivo: demonstration in the human ankle joint and achilles tendon, *Medical engineering & physics* 37 (1) (2015) 93–99.
- [29] C. Sarasaen, S. Chatterjee, M. Breilkopf, G. Rose, A. Nürnbergger, O. Speck, Fine-tuning deep learning model parameters for improved super-resolution of dynamic mri with prior-knowledge, *Artificial Intelligence in Medicine* 121 (2021) 102196.
- [30] S. Chatterjee, C. Sarasaen, G. Rose, A. Nürnbergger, O. Speck, DDos-UNet: Incorporating temporal information using dynamic dual-channel UNet for enhancing super-resolution of dynamic MRI, in: *Medical Imaging with Deep Learning*, 2022.
- [31] V. Arsigny, O. Commowick, N. Ayache, X. Pennec, A fast and log-euclidean polyaffine framework for locally linear registration, *Journal of Mathematical Imaging and Vision* 33 (2) (2009) 222–238.
- [32] V. Arsigny, O. Commowick, X. Pennec, N. Ayache, A log-euclidean polyaffine framework for locally rigid or affine registration, in: *International Workshop on Biomedical Image Registration*, Springer, 2006, pp. 120–127.
- [33] O. Ronneberger, P. Fischer, T. Brox, U-net: Convolutional networks for biomedical image segmentation, in: *International Conference on Medical*



- image computing and computer-assisted intervention, Springer, 2015, pp. 234–241.
- [34] N. M. Brisson, M. Krämer, L. A. Krahl, A. Schill, G. N. Duda, J. R. Reichenbach, A novel multipurpose device for guided knee motion and loading during dynamic magnetic resonance imaging, *Zeitschrift für Medizinische Physik* (2022) S093938892100115Xdoi:10.1016/j.zemedi.2021.12.002.
- [35] S. Klein, M. Staring, K. Murphy, M. A. Viergever, J. P. Pluim, Elastix: a toolbox for intensity-based medical image registration, *IEEE transactions on medical imaging* 29 (1) (2009) 196–205.
- [36] K.-H. Herrmann, M. Krämer, J. R. Reichenbach, Time Efficient 3D Radial UTE Sampling with Fully Automatic Delay Compensation on a Clinical 3T MR Scanner, *PLOS ONE* 11 (3) (2016) 1–16. doi:10.1371/journal.pone.0150371.
- [37] M. Krämer, M. Maggioni, N. M. Brisson, S. Zachow, U. Teichgräber, G. N. Duda, J. R. Reichenbach, T1 and T2\* mapping of the human quadriceps and patellar tendons using ultra-short echo-time (UTE) imaging and bivariate relaxation parameter-based volumetric visualization, *Magnetic resonance imaging* 63 (2019) 29–36.
- [38] G. H. Glover, J. M. Pauly, Projection reconstruction techniques for reduction of motion effects in mri, *Magnetic Resonance in Medicine* 28 (2) (1992) 275–289. arXiv:<https://onlinelibrary.wiley.com/doi/pdf/10.1002/mrm.1910280209>, doi:<https://doi.org/10.1002/mrm.1910280209>.
- [39] D. M. Renz, K.-H. Herrmann, M. Krämer, J. Boettcher, M. Waginger, P.-C. Krüger, A. Pfeil, F. Streitparth, K. Kentouche, B. Gruhn, J. G. Mainz, M. Stenzel, U. K. Teichgräber, J. R. Reichenbach, H.-J. Mentzel, Ultrashort echo time MRI of the lung in children and adolescents: comparison with non-enhanced computed tomography and standard post-contrast T1w MRI sequences, *European Radiology* (Oct. 2021). doi:10.1007/s00330-021-08236-7.
- [40] D. Rückert, L. I. Sonoda, C. Hayes, D. L. Hill, M. O. Leach, D. J. Hawkes, Nonrigid registration using free-form deformations: application

to breast mr images, *IEEE transactions on medical imaging* 18 (8) (1999) 712–721.

- [41] J. Kim, M. M. Matuszak, K. Saitou, J. M. Balter, Distance-preserving rigidity penalty on deformable image registration of multiple skeletal components in the neck, *Medical Physics* 40 (12) (2013) 121907. arXiv:<https://aapm.onlinelibrary.wiley.com/doi/pdf/10.1118/1.4828783>, doi:<https://doi.org/10.1118/1.4828783>.
- [42] F. Isensee, P. F. Jaeger, S. A. A. Kohl, J. Petersen, K. H. Maier-Hein, nnU-Net: a self-configuring method for deep learning-based biomedical image segmentation, *Nat Methods* 18 (2) (2021) 203–211.